Article

Efficient Degradation of Chlortetracycline by Graphene Supported Cobalt Oxide Activated Peroxydisulfate: Performances and Mechanisms

Wei Li [1], Bin Yao [2,*], Yuguo Zheng [1], Guiqiang Zhang [1], Dan Zhi [2] and Yaoyu Zhou [1,2,*]

[1] Key Laboratory of Chemical Synthesis and Environmental Pollution Control-Remediation Technology of Guizhou Province, School of Biology and Chemistry, Minzu Normal University of Xingyi, Xingyi 562400, China; liweiwuxi@126.com (W.L.); yuguozheng@126.com (Y.Z.); guiqiangzhang@126.com (G.Z.)

[2] College of the Environment and Ecology, Hunan Agricultural University, Changsha 410128, China; zhidanvivien@163.com

* Correspondence: binyao121@163.com (B.Y.); zhouyy@hunau.edu.cn (Y.Z.)

Abstract: Cobalt oxide has good catalytic activity for peroxydisulfate (PDS) activation but poor stability and is vulnerable to inactivation because of agglomeration. In this work, the chlortetracycline (CTC) degradation by peroxydisulfate (PDS) catalysis using the reduced graphene oxide support cobalt oxide (Co_3O_4/rGO) composite catalyst was investigated. It was found that 86.3% of CTC was degraded within 120 min in the Co_3O_4/rGO-800/PDS system. The influences of catalyst dosage, PDS concentration, solution pH, and reaction temperature were systematically explored. The excellent removal performance of CTC could be attributed to the synergistic effect between adsorption and catalytic degradation. $\equiv Co^{2+}$ and surface functional groups played as active sites to catalyze PDS, and the circulation of $\equiv Co^{2+}/\equiv Co^{3+}$ was achieved. Moreover, Co_3O_4/rGO-800 showed satisfactory reusability after three cycles. This research can provide useful information for the development of efficient PDS catalysts and facilitate insights into CTC degradation mechanism.

Keywords: antibiotic; advanced oxidation processes (AOPs); reduced graphene oxide; cobalt oxide; wastewater

1. Introduction

Chlortetracycline (CTC) are tetracycline antibiotics that are widely prescribed and often applied as pharmaceutical ingredients and feed additives [1]. Owing to widespread utilization, CTC were detected as common species causing water contamination worldwide [2–4]. When CTC spreads among bacteria and natural microbial populations, it may trigger the imbalance of the ecosystem and threaten human health through the food chain [5]. At the same time, changes in bacterial adaptation caused by the misuse of antibiotics were investigated and evaluated, and the environmental risks posed by the development of drug-resistant bacteria in various countries cannot be underestimated [6,7].

To ensure food safety, control water contamination and the proliferation of drug-resistant bacteria, various approaches were proposed to eliminate CTC [8,9]. Advanced oxidation processes (AOPs) use the powerful oxidative free radicals (such as •OH) to oxidize and even mineralize pollutants, it is considered as an efficient and insightful remediation technique [10]. Recently, sulfate radicals-based AOPs caused rising interests owing to the advantages of high performance and wide operation pH range [11]. Sulfate radicals ($SO_4^{\bullet-}$) could be generated through activating peroxymonosulfate (PMS) and peroxydisulfate (PDS) using different activation strategies, such as UV irradiation, heat, ultrasound, alkaline, and transition metals [12]. Transition metals activation is widely deemed as a promising approach since it is simple, low cost, and high performance [13]. Cobalt (Co) is the most efficient PDS catalyst compared with other transition metals,

and cobalt ion (Co^{2+}) was frequently reported as an effective PDS activator for organic pollutants degradation [14]. However, the application of homogeneous Co^{2+} would lead to the discharge of Co^{2+}. Co^{2+} is highly toxic and carcinogenic, and the remaining Co^{2+} in the aquatic solution are likely to have negative effects on human health [15].

Heterogeneous cobalt containing materials are considered promising alternative approaches. Recently, Co_3O_4 nanoparticles were widely used as PDS catalysts. For instance, Zhang et al. reported that orange G was completely degraded in the Co_3O_4/PDS system in 180 min [16]. Yang et al. investigated the effective degradation of orange G with Co_3O_4 as persulfate catalyst. They found that orange G (30 mg/L) could be almost completely removed after 10 min reaction at 0.5 g/L Co_3O_4 catalyst and 8.0 mM persulfate [17]. However, a serious agglomeration problem was observed when using Co_3O_4 nanoparticles because of the high surface energy [13]. Loading cobalt oxide onto appropriate support materials is a feasible solution to solve this problem [18]. Graphene is a two-dimensional monolayer of sp^2-hybridized carbon material [19]. It is considered as a potential carrier because of large surface area and excellent electrical conductivity [20]. It was reported that the combined transition metals with graphene could improve the stability as well as enhance its catalytic activity [15]. However, graphene will undergo considerable restacking through π–π and hydrophobic–hydrophobic interactions when used directly [21].

Recently, reduced graphene oxide (rGO) exhibited excellent persulfate activation activity for the generation of powerful reactive species [22]. It was reported that the defective structure and ketonic groups existed on rGO might play as active sites for persulfate activation [23]. For example, Olmez-Hanci et al. reported that rGO was an efficient persulfate activator for Bisphenol A degradation. They found that Bisphenol A can be completely removed by rGO/persulfate system within 10 min [23]. Cruz-Alcalde et al. developed the rGO membranes to activate persulfate for phenol and venlafaxine degradation. The results indicated that 90% and 94% of phenol and venlafaxine could be removed after treatment, respectively [24]. Therefore, the integration of rGO with Co_3O_4 nanoparticles can not only improve the dispersive forces within nanomaterial, but the catalyzing activity towards PDS could also be significantly enhanced [25]. For instance, Yan et al. developed reduced graphene oxide supported magnetite nanoparticle composite (nFe_3O_4/rGO) and used it as PDS catalyst for the degradation of trichloroethylene (TCE). The degradation rate of TCE was 98.6% within 5 min at 6.94 g/L of nFe_3O_4/rGO and 3 mM PDS [26]. Ahmad et al. developed reduced graphene oxide-iron nanocomposite (nZVI-rGO) to activate persulfate for trichloroethylene degradation. The results indicated that the nZVI-rGO/persulfate process could remove approximately 99% of trichloroethylene within 2 min [27]. However, there are no researches on the application of rGO-supported cobalt oxide composite as a PDS activator for CTC degradation.

In this work, the CTC degradation by PDS catalysis using the reduced graphene oxide support cobalt oxide (Co_3O_4/rGO) composite catalyst was studied. Co_3O_4/rGO was synthesized with a simple strategy. The crucial influencing factors, including catalyst dosage, PDS concentration, pH, and temperature on CTC degradation, were experimentally explored. CTC degradation mechanisms were investigated according to the experimental results and characterization analysis. The catalyst's reusability was examined using cyclic experiments. The main objectives of this research are to: (1) prepare and systematically characterize the Co_3O_4/rGO-800 catalyst, (2) evaluate the activity of different catalysts that are synthesized under different conditions, (3) investigate the impacts of crucial environmental factors on CTC degradation, (4) elucidate CTC degradation mechanisms in the Co_3O_4/rGO-800/PDS system. This research can provide useful information for the development of efficient PDS catalysts and facilitate insight into CTC degradation mechanism.

2. Materials and Methods

2.1. Chemicals

Urea, $CoCl_2 \bullet 6H_2O$, sodium peroxydisulfate, chlortetracycline hydrochloride (CTC), and NaOH were purchased from Shanghai Macklin Biochemical Co., Ltd., Shanghai, China.

Graphene oxide (GO) was obtained from JCNANO Tech Co., Ltd., Nanjing, China. Ethanol and sulfuric acid was obtained from Sinopharm Chemical Reagent Co., Ltd., Shanghai, China. Deionized (DI) water was used in the experiments.

2.2. Catalysts Synthesis

A total of 50 mg of dried GO was accurately weighed and transferred into a 100 mL beaker. An amount of 20 mL of DI water was added to the beaker, and it was sonicated and dispersed for 30 min to form a GO homogenate. Then, different amounts of $CoCl_2 \bullet 6H_2O$ were added to the homogenate (0.5–2 mM), and 2 g of urea was added to improve the loading success of metal atom. After stirring with an electromagnetic stirrer for 4 h, the homogenate was filtered and thoroughly washed, and dried at 60 °C. The solid was ground into powder form to obtain precursors of the material for subsequent experiments.

The above precursor materials were heated in a tube furnace under N_2 atmosphere at the heating rate of 5 °C min^{-1}. The temperature was set up to reach 700 °C, 800 °C, and 900 °C. Additionally, these temperatures were maintained for 2 h. The black powders were designated Co_3O_4/rGO-700, Co_3O_4/rGO-800, and Co_3O_4/rGO-900.

2.3. Experimental Procedures

CTC degradation was carried out in a 200 mL glass flask containing 100 mL of CTC (20 mg L^{-1}) with a constant stirring at 25 °C. Influences of crucial factors (catalyst dosage, PDS concentration, pH, temperature) were studied using single-factor experiments. A non-homogeneous system was formed by adding 50 mg of catalyst, stirring uniformly and then left to settle for 30 min under light-proof conditions. Then, solution pH was adjusted by using NaOH (1 M) and HCl (1 M). Thereafter, degradation was initiated through adding PDS to the stirred system. At the specified time interval, 1 mL of the sample solution was extracted and filtered through an aqueous microporous membrane (0.45 μm) before the measurement of concentration. The reusability of the catalyst was examined using cycling experiments.

3. Result and Discussion

3.1. Characterization

Scanning electron microscope (SEM) coupling energy dispersive spectrometer (EDS) (ZEISS Sigma 300) was applied for the analysis of surface morphology of catalyst. According to the SEM images (Figure 1a–d), the Co_3O_4/rGO-800 presented an irregular and curled flake structure, which was consistent with the results in other researches [28,29], indicating the reduction in GO was successful. Additionally, the rough and wrinkled surface of graphene flakes increased the effective contact area of the material and exposed more surface active sites, which was significant for the adsorption properties of the Co_3O_4/rGO-800 [23]. In addition, the loading of cobalt was also observed on the surface of the material, and the more uniform spherical or ellipsoidal particles were distributed on the surface of the graphene sheets. According to EDS images (Figure 1e–h), C, N, O, and Co elements were uniformly distributed on the catalyst surface, indicating that reduced graphene oxide-supported cobalt was successfully prepared, which was consistent with the SEM results.

X-ray diffraction (XRD, Panalytical Empyrean) was used to determine the composition of the catalyst. One sharp peak at 2θ = 10.4° attributed to the (001) crystal plane was observed at the XRD pattern of GO (Figure 2) [30]. For Co_3O_4/rGO-800, the peak at 2θ = 10.4° disappeared, and there were three peaks at 2θ = 25.1°, 39.5°, and 49.8°, corresponding to the (002) facet of stacked graphene sheets [28], the (222) and (331) crystal faces of the cobalt oxide (Co_3O_4) nanoparticles, respectively (JCPS No. 76-1802) [31]. These results were in accordance with the SEM results and elemental mapping results. In conclusion, the characterization analysis results demonstrated that cobalt oxide was successfully loaded onto rGO.
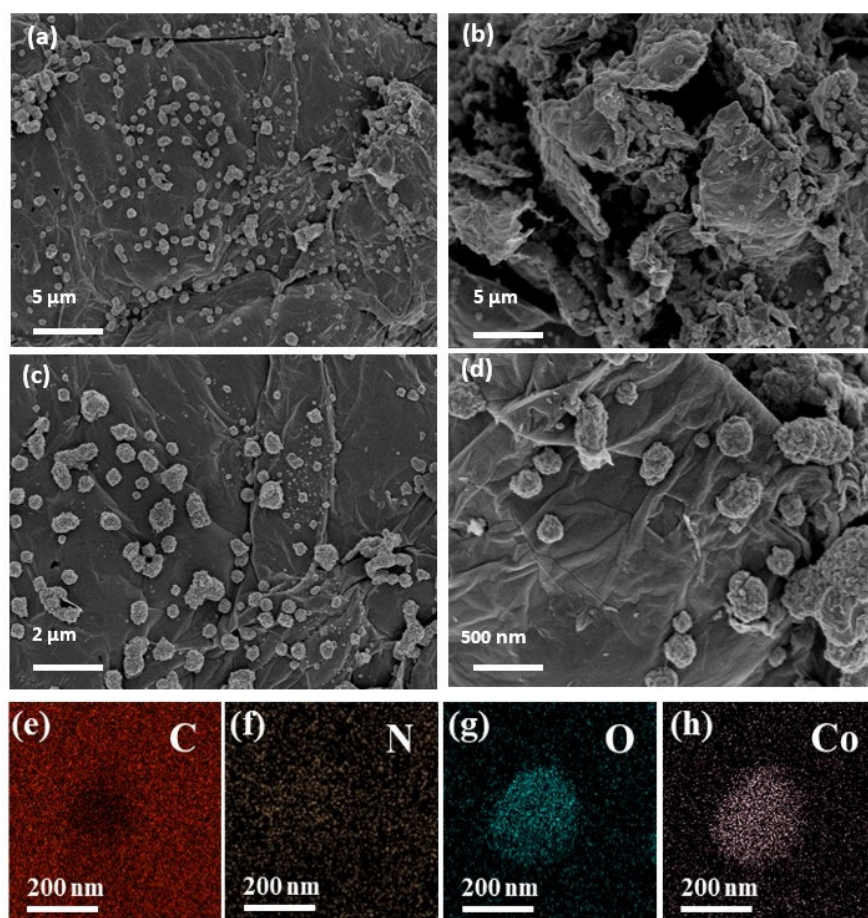
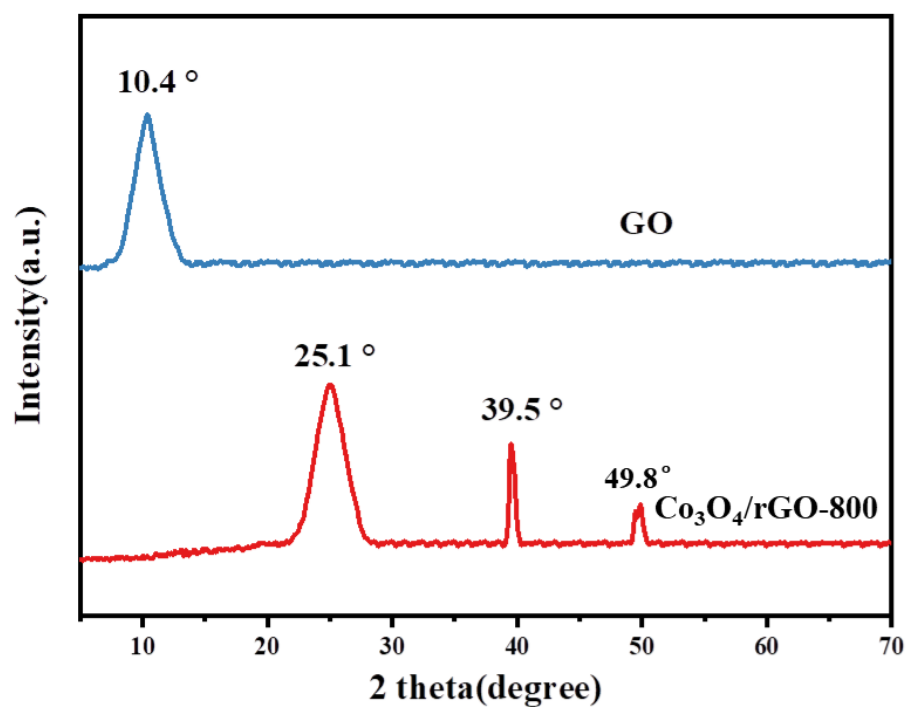**Figure 1.** (**a**–**d**) SEM images of Co_3O_4/rGO-800; (**e**–**h**) the corresponding EDS mapping of Co_3O_4/rGO-800).

Figure 2. XRD patterns of GO and Co_3O_4/rGO-800.

3.2. Evaluation of Catalytic Performance

The catalytic activity of $Co_3O_4/rGO-800$ was evaluated (Figure 3). Clearly, CTC could not be efficiently removed with PDS alone and $Co_3O_4/rGO-800$ alone. Without $Co_3O_4/rGO-800$, only 6.8% of CTC was removed after 120 min, suggesting that CTC could not be efficiently degraded with unactivated PDS, and a catalyst was needed to catalytic reaction [28]. Additionally, the addition of $Co_3O_4/rGO-800$ only removed 23.6% CTC within 120 min. This demonstrated that adsorption was involved in CTC removal process but it was not the predominant mechanism [32]. Meanwhile, CTC degradation efficiency reached 86.3% within 120 min in the $Co_3O_4/rGO-800/PDS$ system. These results clearly demonstrated that CTC removal was mainly driven by the catalytic degradation, and $Co_3O_4/rGO-800$ was a promising PDS catalyst. The enhanced CTC degradation in the $Co_3O_4/rGO-800/PDS$ system might be attributed to the improved physiochemical characteristics after Co loading [33]. In addition, Co species could also play as active sites for PDS activation to generate powerful reactive oxygen species (ROS) [34].
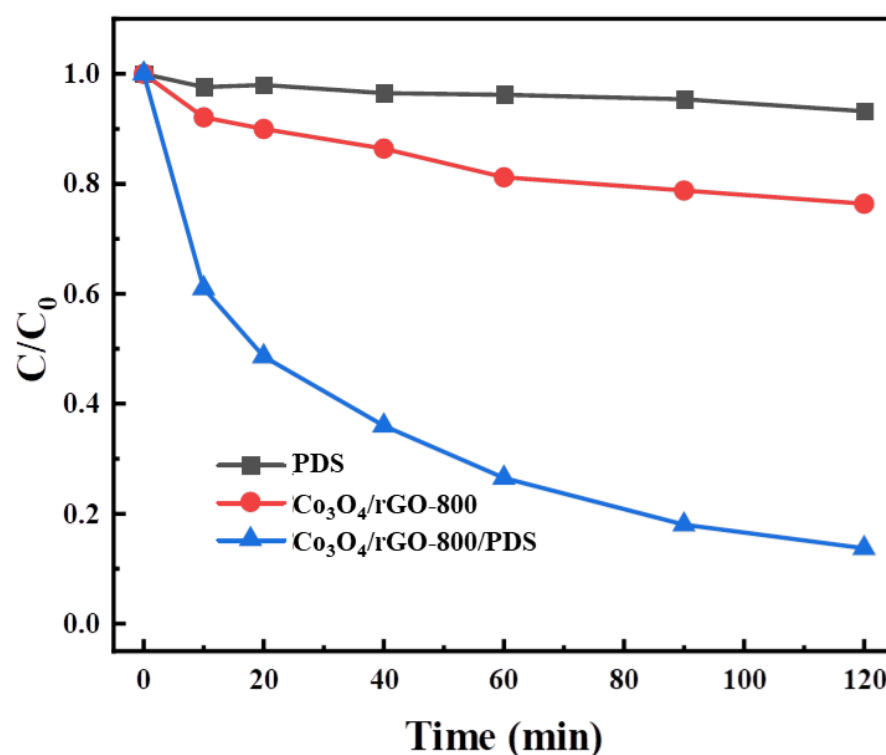

Figure 3. Different reaction systems on the degradation of CTC. (Reaction condition: CTC = 20 mg/L, PDS = 1 g/L, catalyst = 0.5 g/L, T = 25 °C and pH = 5.0).

The experimental result obtained in this research is in accordance with the previous reports. For example, Liu et al. developed carbon-coated Mn_3O_4 nanocube (Mn_3O_4/C) as a persulfate activator for the degradation of 2,4-dichlorophenol (2,4-D). They found that the adsorption removal of 2,4-D by Mn_3O_4/C was about 37%, the direct degradation of 2,4-D by persulfate alone was approximately 26%, and the degradation rate of 2,4-D by $Mn_3O_4/C/PS$ system was 95% [35]. Ren et al. synthesized fishbone-derived biochar (FBBC) as an efficient persulfate catalyst for phenol degradation. They reported that 10.7% of phenol was removed by FBBC adsorption, persulfate could hardly degrade phenol, and the combination of FBBC and persulfate significantly improved phenol removal performances, phenol was completely removed within 60 min in the FBBC/persulfate system [36].

The adsorption of organic pollutants by carbon-based catalyst in persulfate catalyze degradation are very common [37]. The synergistic effect between adsorption and catalyze degradation in sulfate radicals-based AOPs were widely reported previously [38]. In most cases, the adsorption of organic contaminants onto a catalyst's surface is a prerequisite for

persulfate catalysis degradation. In brief, the organic contaminants existing in the reaction matrixes are enriched onto the surface of catalyst. Subsequently, the active sites on the catalyst can catalyze persulfate to generate surface-bound reactive oxygen species ($\bullet OH$ and $SO_4^{\bullet-}$). Then, the adsorbed organic pollutants are rapidly degraded by the attached reactive oxygen species [39]. Therefore, there is no doubt that both adsorption and catalyzed degradation contributed to CTC removal, and this conclusion was not only supported by the experimental results, but it could also be justified by the related scientific references.

The effect of calcination temperatures on the activation activity of Co_3O_4/rGO catalyst was investigated (Figure 4a). When pyrolysis temperature increased from 700 °C to 800 °C, CTC degradation efficiency increased from 76.03% to 86.3%. This might be attributed to the formation of higher sp^2 carbon contents under high pyrolysis temperature [40]. However, as the calcination temperature further increased from 800 °C to 900 °C, CTC degradation rate declined from 86.3% to 78.97%. The collapse of carbon structure could be caused at excessively high pyrolysis temperature, and then, limit the catalytic activity [41]. Additionally, PDS activation and CTC degradation reactions occurred at the surface of catalyst, the adsorption of PDS and CTC onto the surface of catalyst is the prerequisite for CTC degradation [32]. The collapse of carbon skeleton would decrease the pore sizes and surface areas of catalysts, and the adsorption performances would be negatively affected [41]. Based on this, a catalyst calcined at 800 °C was selected for the subsequent experiments.

The effect of Co on the catalytic performance was systematically explored with catalyst synthesized using different amounts of Co for CTC degradation (Figure 4b). It could be found that CTC degradation efficiency enhanced with Co content increasing, and the degradation rate enhanced from 67.91% to 87.2% when the amount of Co increased from 0.5 mmol to 2 mmol. This suggested that the catalytic ability of Co_3O_4/rGO could be improved through the addition of an appropriate amount of Co; therefore, the CTC degradation efficiency was enhanced [42]. In addition, CTC degradation performance increased slightly from 86.3% to 87.2% when the Co content increased from 1 mmol to 2 mmol. This might be because of the aggregation of nanomaterial [43]. Thus, 1 mmol was adopted for the subsequent experiments.

3.3. Influence of Reaction Parameters

3.3.1. Dosage of Catalyst

Figure 4c illustrated the influence of catalyst dosage on CTC degradation. Clearly, CTC degradation improved with the increase in catalyst dosage. When the Co_3O_4/rGO-800 dosage was 0.2 g/L, CTC degradation ratio was 57.9% within 120 min. As the dosage increased from 0.2 g/L to 0.5 g/L, CTC degradation significantly enhanced from 57.9% to 86.3%. This implied that the increase in catalyst dosage resulted in more active sites to catalyze PDS for CTC degradation [43]. However, it was reported that the degradation rate would not enhance significantly when the catalyst dosage further increased to a certain amount, which might be explained by the fact that the active sites were enough for PDS catalysis [44]. Consequently, the optimal dosage for Co_3O_4/rGO-800 was 0.5 g/L.

3.3.2. PDS Concentration

In Fenton-like reaction systems, apart from the amount of catalyst, the amount of oxidant was equally important. The influence of PDS concentration on CTC degradation was explored. As seen in Figure 4d, as the concentration of PDS gradually increased from 0.5 g/L to 2 g/L, the degradation rate markedly improved from 59.1% to 88.0%. It can be seen that the greater the dosage of PDS in a certain range, the more obvious the effect. At the same time, it can also be observed that there was no significant difference in the degradation ratio when PDS concentration increased from 1 g/L to 2 g/L, which might be explained that the excessive PDS would result in the self-quenching effect (Equations (1) and (2)) [45]. In addition, the excessive PDS would compete with CTC for the adsorption active sites on the surface of Co_3O_4/rGO-800 catalyst [32]. So, 1.0 g/L PDS was selected as the optimal concentration.

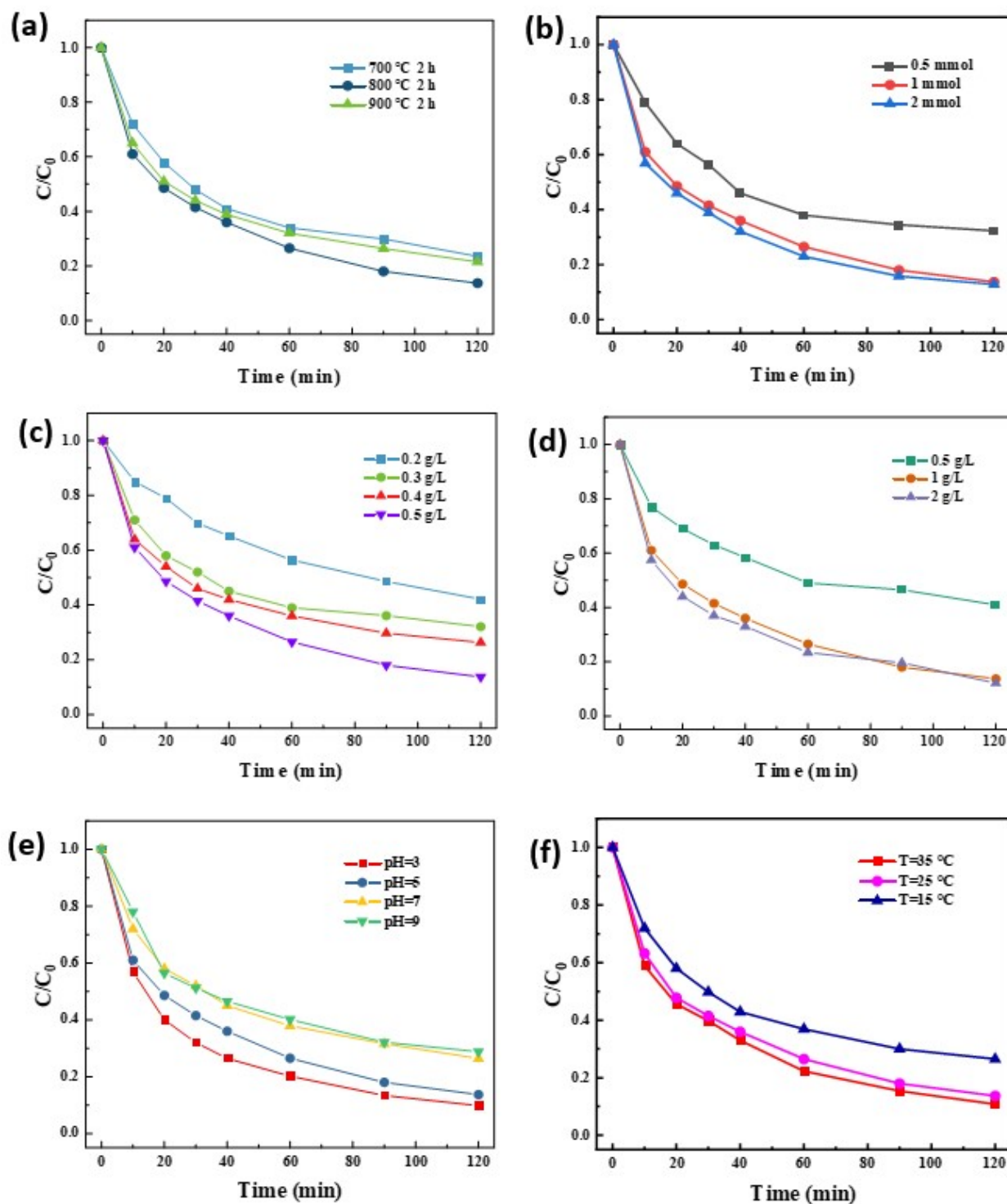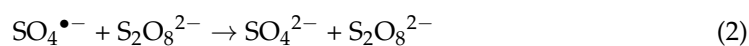**Figure 4.** Influences of (**a**) calcination temperature, (**b**) Co loading amounts, (**c**) dosage of Co$_3$O$_4$/rGO-800, (**d**) concentration of PDS, (**e**) initial pH, (**f**) reaction temperature on the degradation of CTC. (Reaction condition: CTC = 20 mg/L, PDS = 0.5–2.0 g/L, catalyst = 0.2–0.5 g/L, T = 15–35 °C, and pH = 3–9).

$$SO_4{}^{\bullet-} + SO_4{}^{\bullet-} \rightarrow S_2O_8{}^{2-} \tag{1}$$

$$SO_4{}^{\bullet-} + S_2O_8{}^{2-} \rightarrow SO_4{}^{2-} + S_2O_8{}^{2-} \tag{2}$$

3.3.3. Solution pH

Solution pH could significantly affect the surface charge of catalyst [46,47], leach of metal ions [32], ionization of CTC [48], and PDS activation [12]; thus, the impact of solution pH on CTC degradation was explored. As depicted in Figure 4e, CTC degradation rate reached the highest at pH 3 (90.2%), and it gradually declined to 71.2% when pH increased from 3 to 9. The results were in line with the previous reports [45,49]. The ineffective consumption of $SO_4^{\bullet-}$ and $\bullet OH$ under high pH conditions might be a major reason responsible for the decreased CTC degradation efficiency (Equations (3)–(6)) [49]. In addition, CTC is an amphiphilic molecule, the pK_a values for CTC were pK_{a1} = 3.3, pK_{a2} = 7.44, pK_{a3} = 9.5. CTC was negatively charged (CTC^- and CTC^{2-}) at high pH conditions, and positively charged (CTC^+) under acidic condition [50]. The surface of Co_3O_4/rGO-800 was positively charged at acidic condition like other carbon materials [51,52]; therefore, it was expected that the strong electrostatic repulsion could occur between CTC and Co_3O_4/rGO-800. The excellent CTC degradation performances might because the leached Co^{2+} promoted PDS activation through homogenous catalysis [32]. However, 71.2% of CTC was degraded at pH 9 in the Co_3O_4/rGO-800/PDS system, demonstrating that the Co_3O_4/rGO-800/PDS system could remain high stability at a wide range of pH.

$$SO_4^{\bullet-} + H_2O \rightarrow HSO_4^- + \bullet OH \tag{3}$$

$$SO_4^{\bullet-} + OH^- \rightarrow SO_4^{2-} + \bullet OH \tag{4}$$

$$\bullet OH + \bullet OH \rightarrow H_2O_2 \tag{5}$$

$$S_2O_8^{2-} + H_2O_2 \rightarrow 2\,SO_4^{2-} + O_2 \tag{6}$$
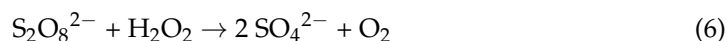
3.3.4. Reaction Temperature

Temperature was also considered as an important factor. The effect of solution temperature (T = 15 °C, 25 °C and 35 °C) on CTC degradation was studied. As revealed in Figure 4f, the optimal degradation effect was achieved when the solution temperature was 35 °C, reaching 89.2% in 120 min. With the solution temperature gradually decreased from 35 °C to 15 °C, the degradation rate also decreased from 89.2% to 73.5%, which demonstrated that the system had a good degradation effect on CTC under a wide range of temperatures. The temperature accelerated the movement of molecules and the contact between the catalyst and PDS was more frequent, which promoted the faster generation of free radicals and the corresponding increase in the degradation rate of CTC [53].

3.4. Reusability of Catalyst

The durability and reusability of the Co_3O_4/rGO-800 catalyst were significant indicators to be considered in practical applications. Recyclable materials will considerably reduce disposal costs and lower costs [54]. As displayed in Figure 5, the degradation rates of CTC reached 86.3%, 71.1%, and 63.7% in the first, second, and third cycle tests, respectively. The decrease in degradation rate in the second and third cycles was presumed because the active sites of the material were worn out or consumed during the previous experiments and part of the structure was destroyed, which led to the decrease in catalytic effect [32]. However, the removal rate in the third cycle was still higher than the related previous paper. For example, Su et al. developed graphene oxide-carbon nanotubes anchored α-FeOOH hybrid catalyst (α-FeOOH@GCA) as a persulfate activator for the degradation of Orange II. The degradation rate obtained in the first run in the α-FeOOH@GCA/persulfate system was 99.1%, and the rate then decreased to 38.4% in the third cycle [55]. Pedrosa et al. prepared metal-free graphene-based catalytic membrane for persulfate activation to degrade phenol, they found that the degradation rate decreased from 94% to 27% after three cyclic experiments [30]. Olmez-Hanci et al. reported the degradation of Bisphenol A by reduced graphene oxide (rGO)/persulfate system. In the first run, Bisphenol A can be completely removed within 10 min. Additionally, the degradation rate gradually decreased to 68%,

33%, and 35% in the second, third, and fourth cycles after 30 min reaction, respectively [23]. Jiang et al. developed graphene-like carbon sheet supported nanoscale zero-valent iron (nZVI@CS) as a persulfate catalyst for the degradation of atrazine. The removal ratio of atrazine in the nZVI@CS/persulfate system was 84.27% in the first run, and then, it decreased to 82.0%, 63.1%, and 14.2% in the second, third, and fourth cycles, respectively [38]. Therefore, the as-synthesized Co3O4/rGO-800 catalyst was superior or comparable to the previous related papers. Additionally, it exhibited good stability and reusability in cyclic experiments. In fact, the decline in the catalyze reactivity of the carbon-based catalyst in sulfate radicals-based AOPs is very common, and it was extensively reported. Leaching of metal species, consumption of active sites, and the destruction of structure might all contribute to the decreased catalytic reactivity [56]. To further increase the stability of the catalyst, great efforts should be dedicated in future research.
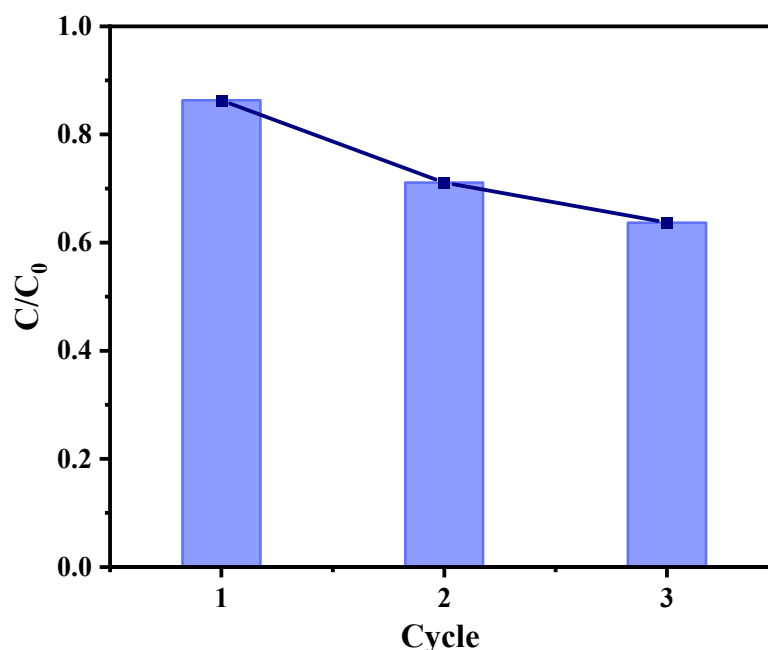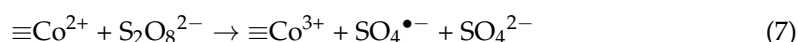

Figure 5. Cyclic degradation of CTC by the recycled $Co_3O_4/rGO-800$ (reaction condition: CTC = 20 mg/L, PDS = 1 g/L, catalyst = 0.5 g/L, T = 25 °C, and pH = 5.0). 3.5. Proposed degradation mechanisms.

According to the aforementioned results, CTC degradation mechanisms in the $Co_3O_4/$ rGO-800/PDS system were concluded (Figure 6). Generally, CTC removal in the Co_3O_4/rG O-800/PDS system could be attributed the synergistic effect between adsorption and catalyze oxidation. The predominant mechanism that was responsible for CTC removal was the catalyzed oxidation. Firstly, PDS and CTC were adsorbed onto the surface of $Co_3O_4/rGO-800$ catalyst. Thereafter, PDS was activated by the active sites existing on $Co_3O_4/rGO-800$ material to generate powerful radicals including $\bullet OH$ and $SO_4^{\bullet-}$. $\equiv Co^{2+}$ and surface functional groups played as active sites for PDS catalysis (Equations (7) and (8)) [11,57]. Meanwhile, $\equiv Co^{2+}$ could be regenerated during the reaction, and the circulation of $\equiv Co^{2+}/\equiv Co^{3+}$ was achieved (Equations (9) and (10)) [58]. CTC was finally decomposed by powerful oxidative radicals to form small molecule compounds with less toxic.
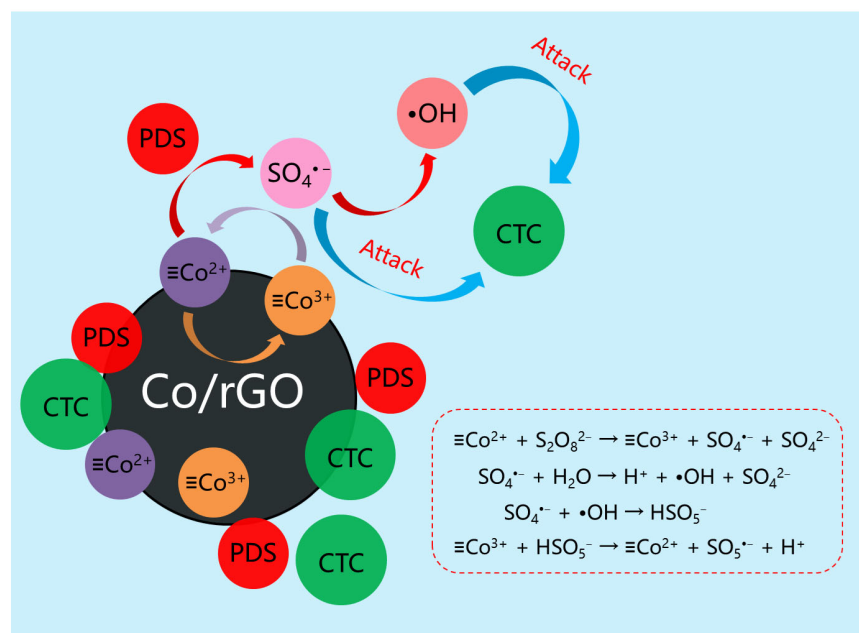
$$\equiv Co^{2+} + S_2O_8^{2-} \rightarrow \equiv Co^{3+} + SO_4^{\bullet-} + SO_4^{2-} \tag{7}$$

$$SO_4^{\bullet-} + H_2O \rightarrow H^+ + \bullet OH + SO_4^{2-} \tag{8}$$

$$SO_4^{\bullet-} + \bullet OH \rightarrow HSO_5^- \tag{9}$$

$$\equiv Co^{3+} + HSO_5^- \rightarrow \equiv CO^{2+} + SO_5^{\bullet-} + H^+ \tag{10}$$

Figure 6. Proposed mechanism for CTC degradation in the Co/rGO/PS system.

4. Conclusions

In the present research, reduced graphene supported cobalt oxide (Co_3O_4/rGO) catalyst was successfully synthesized using a simple strategy to catalyze persulfate (PDS) for the degradation of chlortetracycline (CTC). The Co_3O_4/rGO-800 presented an irregular and curled flake structure, large surface area, and abundant functional groups, which provided an excellent degradation performance for CTC (86.3% in 120 min). The excellent catalyze ability of Co/rGO material could be attributed to the synergistic effect between graphene and cobalt oxide. The study showed that both adsorption and catalyzed oxidation were involved in the removal process, and catalyze oxidation was the predominant mechanism. PDS was activated by the active sites (cobalt oxide and oxygen-containing functional groups) on the surface of Co_3O_4/rGO-800 catalyst, and the generated powerful radicals ($SO_4^{\bullet -}$ and $\bullet OH$) could attack CTC into byproducts with less toxic. Co_3O_4/rGO-800 showed good stability in the cyclic experiments (63.7% removal of CTC after 3 cycles of reuse). This research demonstrated the practical application potential of Co_3O_4/rGO as a PDS catalyst material with the advantages of simple production process and high catalytic performance. This work could provide a scientific basis for the future development and research of environmentally functional materials applied in wastewater treatment.

Author Contributions: Conceptualization, Y.Z. (Yaoyu Zhou); methodology, Y.Z. (Yuguo Zheng); software, G.Z.; Validation, W.L.; formal analysis, W.L.; investigation, Y.Z. (Yuguo Zheng), G.Z., and W.L.; resources, Y.Z. (Yaoyu Zhou); data curation, W.L., Y.Z. (Yuguo Zheng), and G.Z.; writing—original draft preparation, W.L.; writing—review and editing, W.L., B.Y., D.Z., and Y.Z. (Yaoyu Zhou); visualization, W.L. and B.Y.; supervision, W.L. and Y.Z. (Yaoyu Zhou); project administration, W.L. and Y.Z. (Yaoyu Zhou); funding acquisition, W.L. and Y.Z. (Yaoyu Zhou). All authors have read and agreed to the published version of the manuscript.

Informed Consent Statement: Not applicable.

Data Availability Statement: Data used in this work are available on reasonable request.

Conflicts of Interest: The authors declare no competing interests.

References

1. Chen, Y.-P.; Zheng, C.-H.; Huang, Y.-Y.; Chen, Y.-R. Removal of chlortetracycline from water using spent tea leaves-based biochar as adsorption-enhanced persulfate activator. *Chemosphere* **2022**, *286*, 131770. [CrossRef] [PubMed]
2. Leng, Y.; Xiao, H.; Li, Z.; Wang, J. Tetracyclines, sulfonamides and quinolones and their corresponding resistance genes in coastal areas of Beibu Gulf, China. *Sci. Total Environ.* **2020**, *714*, 136899. [CrossRef] [PubMed]
3. Liu, L.; Liu, Y.-H.; Wang, Z.; Liu, C.-X.; Huang, X.; Zhu, G.-F. Behavior of tetracycline and sulfamethazine with corresponding resistance genes from swine wastewater in pilot-scale constructed wetlands. *J. Hazard. Mater.* **2014**, *278*, 304–310. [CrossRef] [PubMed]
4. Yan, M.; Xu, C.; Huang, Y.; Nie, H.; Wang, J. Tetracyclines, sulfonamides and quinolones and their corresponding resistance genes in the Three Gorges Reservoir, China. *Sci. Total Environ.* **2018**, *631–632*, 840–848. [CrossRef]
5. Martinez, J.L. Environmental pollution by antibiotics and by antibiotic resistance determinants. *Environ. Pollut.* **2009**, *157*, 2893–2902. [CrossRef]
6. Gao, R.; Sui, M. Antibiotic resistance fate in the full-scale drinking water and municipal wastewater treatment processes: A review. *Environ. Eng. Res.* **2021**, *26*, 200324. [CrossRef]
7. Sabri, N.A.; Schmitt, H.; Van der Zaan, B.; Gerritsen, H.W.; Zuidema, T.; Rijnaarts, H.H.M.; Langenhoff, A.A.M. Prevalence of antibiotics and antibiotic resistance genes in a wastewater effluent-receiving river in the Netherlands. *J. Environ. Chem. Eng.* **2020**, *8*, 102245. [CrossRef]
8. Wang, J.; Wang, S. Removal of pharmaceuticals and personal care products (PPCPs) from wastewater: A review. *J. Environ. Manag.* **2016**, *182*, 620–640. [CrossRef]
9. Yao, B.; Luo, Z.; Yang, J.; Zhi, D.; Zhou, Y. FeIIFeIII layered double hydroxide modified carbon felt cathode for removal of ciprofloxacin in electro-Fenton process. *Environ. Res.* **2021**, *197*, 111144. [CrossRef]
10. Wang, J.; Zhuan, R. Degradation of antibiotics by advanced oxidation processes: An overview. *Sci. Total Environ.* **2020**, *701*, 135023. [CrossRef]
11. Guan, R.; Yuan, X.; Wu, Z.; Jiang, L.; Zhang, J.; Li, Y.; Zeng, G.; Mo, D. Efficient degradation of tetracycline by heterogeneous cobalt oxide/cerium oxide composites mediated with persulfate. *Sep. Purif. Technol.* **2019**, *212*, 223–232. [CrossRef]
12. Wang, J.; Wang, S. Activation of persulfate (PS) and peroxymonosulfate (PMS) and application for the degradation of emerging contaminants. *Chem. Eng. J.* **2018**, *334*, 1502–1517. [CrossRef]
13. Jiang, Z.; Zhao, J.; Li, C.; Liao, Q.; Xiao, R.; Yang, W. Strong synergistic effect of Co_3O_4 encapsulated in nitrogen-doped carbon nanotubes on the nonradical-dominated persulfate activation. *Carbon* **2020**, *158*, 172–183. [CrossRef]
14. Hu, P.; Long, M. Cobalt-catalyzed sulfate radical-based advanced oxidation: A review on heterogeneous catalysts and applications. *Appl. Catal. B Environ.* **2016**, *181*, 103–117. [CrossRef]
15. Li, B.; Wang, Y.-F.; Zhang, L.; Xu, H.-Y. Enhancement strategies for efficient activation of persulfate by heterogeneous cobalt-containing catalysts: A review. *Chemosphere* **2022**, *291*, 132954. [CrossRef]
16. Zhang, J.; Chen, M.; Zhu, L. Activation of persulfate by Co_3O_4 nanoparticles for orange G degradation. *RSC Adv.* **2016**, *6*, 758–768. [CrossRef]
17. Yang, W.; Li, X.; Jiang, Z.; Li, C.; Zhao, J.; Wang, H.; Liao, Q. Structure-dependent catalysis of Co_3O_4 crystals in persulfate activation via nonradical pathway. *Appl. Surf. Sci.* **2020**, *525*, 146482. [CrossRef]
18. Wu, S.; Yang, D.; Zhou, Y.; Zhou, H.; Ai, S.; Yang, Y.; Wan, Z.; Luo, L.; Tang, L.; Tsang, D.C.W. Simultaneous degradation of p-arsanilic acid and inorganic arsenic removal using M-rGO/PS Fenton-like system under neutral conditions. *J. Hazard. Mater.* **2020**, *399*, 123032. [CrossRef]
19. Xu, L.; Wang, J. The application of graphene-based materials for the removal of heavy metals and radionuclides from water and wastewater. *Crit. Rev. Environ. Sci. Technol.* **2017**, *47*, 1042–1105. [CrossRef]
20. Bekris, L.; Frontistis, Z.; Trakakis, G.; Sygellou, L.; Galiotis, C.; Mantzavinos, D. Graphene: A new activator of sodium persulfate for the advanced oxidation of parabens in water. *Water Res.* **2017**, *126*, 111–121. [CrossRef]
21. Agarwal, V.; Zetterlund, P.B. Strategies for reduction of graphene oxide—A comprehensive review. *Chem. Eng. J.* **2021**, *405*, 127018. [CrossRef]
22. Wang, Q.; Li, L.; Luo, L.; Yang, Y.; Yang, Z.; Li, H.; Zhou, Y. Activation of persulfate with dual-doped reduced graphene oxide for degradation of alkylphenols. *Chem. Eng. J.* **2019**, *376*, 120891. [CrossRef]
23. Olmez-Hanci, T.; Arslan-Alaton, I.; Gurmen, S.; Gafarli, I.; Khoei, S.; Safaltin, S.; Ozcelik, D.Y. Oxidative degradation of Bisphenol A by carbocatalytic activation of persulfate and peroxymonosulfate with reduced graphene oxide. *J. Hazard. Mater.* **2018**, *360*, 141–149. [CrossRef] [PubMed]
24. Cruz-Alcalde, A.; López-Vinent, N.; Ribeiro, R.S.; Giménez, J.; Sans, C.; Silva, A.M.T. Persulfate activation by reduced graphene oxide membranes: Practical and mechanistic insights concerning organic pollutants abatement. *Chem. Eng. J.* **2022**, *427*, 130994. [CrossRef]
25. Chen, Y.; Bai, X.; Ji, Y.; Shen, T. Reduced graphene oxide-supported hollow Co_3O_4@N-doped porous carbon as peroxymonosulfate activator for sulfamethoxazole degradation. *Chem. Eng. J.* **2022**, *430*, 132951. [CrossRef]
26. Yan, J.; Gao, W.; Dong, M.; Han, L.; Qian, L.; Nathanail, C.P.; Chen, M. Degradation of trichloroethylene by activated persulfate using a reduced graphene oxide supported magnetite nanoparticle. *Chem. Eng. J.* **2016**, *295*, 309–316. [CrossRef]

27. Ahmad, A.; Gu, X.; Li, L.; Lv, S.; Xu, Y.; Guo, X. Efficient degradation of trichloroethylene in water using persulfate activated by reduced graphene oxide-iron nanocomposite. *Environ. Sci. Pollut. Res.* **2015**, *22*, 17876–17885. [CrossRef]

28. Fan, M.; Zhang, P.; Wang, C.; Tang, J.; Sun, H. Tailored design of three-dimensional rGOA-nZVI catalyst as an activator of persulfate for degradation of organophosphorus pesticides. *J. Hazard. Mater.* **2022**, *428*, 128254. [CrossRef]

29. Zuo, S.; Jin, X.; Wang, X.; Lu, Y.; Zhu, Q.; Wang, J.; Liu, W.; Du, Y.; Wang, J. Sandwich structure stabilized atomic Fe catalyst for highly efficient Fenton-like reaction at all pH values. *Appl. Catal. B Environ.* **2021**, *282*, 119551. [CrossRef]

30. Pedrosa, M.; Drazic, G.; Tavares, P.B.; Figueiredo, J.L.; Silva, A.M.T. Metal-free graphene-based catalytic membrane for degradation of organic contaminants by persulfate activation. *Chem. Eng. J.* **2019**, *369*, 223–232. [CrossRef]

31. Anuma, S.; Mishra, P.; Bhat, B.R. Polypyrrole functionalized Cobalt oxide Graphene (COPYGO) nanocomposite for the efficient removal of dyes and heavy metal pollutants from aqueous effluents. *J. Hazard. Mater.* **2021**, *416*, 125929. [CrossRef]

32. Yao, B.; Luo, Z.; Du, S.; Yang, J.; Zhi, D.; Zhou, Y. Magnetic $MgFe_2O_4$/biochar derived from pomelo peel as a persulfate activator for levofloxacin degradation: Effects and mechanistic consideration. *Bioresour. Technol.* **2022**, *346*, 126547. [CrossRef]

33. Yao, B.; Chen, X.; Zhou, K.; Luo, Z.; Li, P.; Yang, Z.; Zhou, Y. p-Arsanilic acid decontamination over a wide pH range using biochar-supported manganese ferrite material as an effective persulfate catalyst: Performances and mechanisms. *Biochar* **2022**, *4*, 31. [CrossRef]

34. Liang, X.; Wang, D.; Zhao, Z.; Li, T.; Chen, Z.; Gao, Y.; Hu, C. Engineering the low-coordinated single cobalt atom to boost persulfate activation for enhanced organic pollutant oxidation. *Appl. Catal. B Environ.* **2022**, *303*, 120877. [CrossRef]

35. Liu, Y.; Luo, J.; Tang, L.; Feng, C.; Wang, J.; Deng, Y.; Liu, H.; Yu, J.; Feng, H.; Wang, J. Origin of the Enhanced Reusability and Electron Transfer of the Carbon-Coated Mn_3O_4 Nanocube for Persulfate Activation. *ACS Catal.* **2020**, *10*, 14857–14870. [CrossRef]

36. Ren, X.; Wang, J.; Yu, J.; Song, B.; Feng, H.; Shen, M.; Zhang, H.; Zou, J.; Zeng, G.; Tang, L.; et al. Waste valorization: Transforming the fishbone biowaste into biochar as an efficient persulfate catalyst for degradation of organic pollutant. *J. Clean. Prod.* **2021**, *291*, 125225. [CrossRef]

37. Chen, X.; Oh, W.-D.; Lim, T.-T. Graphene- and CNTs-based carbocatalysts in persulfates activation: Material design and catalytic mechanisms. *Chem. Eng. J.* **2018**, *354*, 941–976. [CrossRef]

38. Jiang, Q.; Zhang, Y.; Jiang, S.; Wang, Y.; Li, H.; Han, W.; Qu, J.; Wang, L.; Hu, Y. Graphene-like carbon sheet-supported nZVI for efficient atrazine oxidation degradation by persulfate activation. *Chem. Eng. J.* **2021**, *403*, 126309. [CrossRef]

39. Wang, X.; Qin, Y.; Zhu, L.; Tang, H. Nitrogen-Doped Reduced Graphene Oxide as a Bifunctional Material for Removing Bisphenols: Synergistic Effect between Adsorption and Catalysis. *Environ. Sci. Technol.* **2015**, *49*, 6855–6864. [CrossRef]

40. Shang, Y.; Chen, C.; Zhang, P.; Yue, Q.; Li, Y.; Gao, B.; Xu, X. Removal of sulfamethoxazole from water via activation of persulfate by Fe_3C@NCNTs including mechanism of radical and nonradical process. *Chem. Eng. J.* **2019**, *375*, 122004. [CrossRef]

41. Li, X.; Liao, F.; Ye, L.; Yeh, L. Controlled pyrolysis of MIL-88A to prepare iron/carbon composites for synergistic persulfate oxidation of phenol: Catalytic performance and mechanism. *J. Hazard. Mater.* **2020**, *398*, 122938. [CrossRef] [PubMed]

42. Liu, Z.; Pan, S.; Xu, F.; Wang, Z.; Zhao, C.; Xu, X.; Gao, B.; Li, Q. Revealing the fundamental role of MoO_2 in promoting efficient and stable activation of persulfate by iron carbon based catalysts: Efficient Fe^{2+}/Fe^{3+} cycling to generate reactive species. *Water Res.* **2022**, *225*, 119142. [CrossRef] [PubMed]

43. Zhu, K.; Bin, Q.; Shen, Y.; Huang, J.; He, D.; Chen, W. In-situ formed N-doped bamboo-like carbon nanotubes encapsulated with Fe nanoparticles supported by biochar as highly efficient catalyst for activation of persulfate (PS) toward degradation of organic pollutants. *Chem. Eng. J.* **2020**, *402*, 126090. [CrossRef]

44. Chen, L.; Jiang, X.; Xie, R.; Zhang, Y.; Jin, Y.; Jiang, W. A novel porous biochar-supported Fe-Mn composite as a persulfate activator for the removal of acid red 88. *Sep. Purif. Technol.* **2020**, *250*, 117232. [CrossRef]

45. Ma, D.; Yang, Y.; Liu, B.; Xie, G.; Chen, C.; Ren, N.; Xing, D. Zero-valent iron and biochar composite with high specific surface area via K_2FeO_4 fabrication enhances sulfadiazine removal by persulfate activation. *Chem. Eng. J.* **2021**, *408*, 127992. [CrossRef]

46. Yao, B.; Luo, Z.; Du, S.; Yang, J.; Zhi, D.; Zhou, Y. Sustainable biochar/$MgFe_2O_4$ adsorbent for levofloxacin removal: Adsorption performances and mechanisms. *Bioresour. Technol.* **2021**, *340*, 125698. [CrossRef]

47. Yao, B.; Li, Y.; Zeng, W.; Yang, G.; Zeng, J.; Nie, J.; Zhou, Y. Synergistic adsorption and oxidation of trivalent antimony from groundwater using biochar supported magnesium ferrite: Performances and mechanisms. *Environ. Pollut.* **2023**, *323*, 121318. [CrossRef]

48. Ma, Y.; Li, M.; Li, P.; Yang, L.; Wu, L.; Gao, F.; Qi, X.; Zhang, Z. Hydrothermal synthesis of magnetic sludge biochar for tetracycline and ciprofloxacin adsorptive removal. *Bioresour. Technol.* **2021**, *319*, 124199. [CrossRef]

49. Ouyang, D.; Yan, J.; Qian, L.; Chen, Y.; Han, L.; Su, A.; Zhang, W.; Ni, H.; Chen, M. Degradation of 1,4-dioxane by biochar supported nano magnetite particles activating persulfate. *Chemosphere* **2017**, *184*, 609–617. [CrossRef]

50. Taheran, M.; Naghdi, M.; Brar, S.K.; Knystautas, E.J.; Verma, M.; Ramirez, A.A.; Surampalli, R.Y.; Valero, J.R. Adsorption study of environmentally relevant concentrations of chlortetracycline on pinewood biochar. *Sci. Total Environ.* **2016**, *571*, 772–777. [CrossRef]

51. Ma, Y.; Lu, T.; Tang, J.; Li, P.; Mašek, O.; Yang, L.; Wu, L.; He, L.; Ding, Y.; Gao, F.; et al. One-pot hydrothermal synthesis of magnetic N-doped sludge biochar for efficient removal of tetracycline from various environmental waters. *Sep. Purif. Technol.* **2022**, *297*, 121426. [CrossRef]

52. Xiong, W.; Zeng, Z.; Li, X.; Zeng, G.; Xiao, R.; Yang, Z.; Zhou, Y.; Zhang, C.; Cheng, M.; Hu, L.; et al. Multi-walled carbon nanotube/amino-functionalized MIL-53(Fe) composites: Remarkable adsorptive removal of antibiotics from aqueous solutions. *Chemosphere* **2018**, *210*, 1061–1069. [CrossRef]

53. Yao, B.; Luo, Z.; Zhi, D.; Hou, D.; Luo, L.; Du, S.; Zhou, Y. Current progress in degradation and removal methods of polybrominated diphenyl ethers from water and soil: A review. *J. Hazard. Mater.* **2021**, *403*, 123674. [CrossRef]

54. Luo, Z.; Yao, B.; Yang, X.; Wang, L.; Xu, Z.; Yan, X.; Tian, L.; Zhou, H.; Zhou, Y. Novel insights into the adsorption of organic contaminants by biochar: A review. *Chemosphere* **2022**, *287*, 132113. [CrossRef]

55. Su, S.; Liu, Y.; He, W.; Tang, X.; Jin, W.; Zhao, Y. A novel graphene oxide-carbon nanotubes anchored α-FeOOH hybrid activated persulfate system for enhanced degradation of Orange II. *J. Environ. Sci.* **2019**, *83*, 73–84. [CrossRef]

56. Lu, J.; Zhou, Y.; Lei, J.; Ao, Z.; Zhou, Y. Fe_3O_4/graphene aerogels: A stable and efficient persulfate activator for the rapid degradation of malachite green. *Chemosphere* **2020**, *251*, 126402. [CrossRef]

57. Xian, G.; Zhang, G.; Chang, H.; Zhang, Y.; Zou, Z.; Li, X. Heterogeneous activation of persulfate by Co_3O_4-CeO_2 catalyst for diclofenac removal. *J. Environ. Manag.* **2019**, *234*, 265–272. [CrossRef]

58. Jiang, Z.; Wei, J.; Zhang, Y.; Niu, X.; Li, J.; Li, Y.; Pan, G.; Xu, M.; Cui, X.; Cui, N.; et al. Electron transfer mechanism mediated nitrogen-enriched biochar encapsulated cobalt nanoparticles catalyst as an effective persulfate activator for doxycycline removal. *J. Clean. Prod.* **2023**, *384*, 135641. [CrossRef]